Roles of Electric Field and Fiber Structure in Cardiac Electric Stimulation

Stephen B. Knisley,* Natalia Trayanova,# and Felipe Aguel#

*Department of Biomedical Engineering of the School of Engineering, The University of Alabama at Birmingham, Alabama 35294, and #Department of Biomedical Engineering of the School of Engineering, Tulane University, New Orleans, Louisiana USA

ABSTRACT This study investigated roles of the variation of extracellular voltage gradient (VG) over space and cardiac fibers in production of transmembrane voltage changes (ΔV_m) during shocks. Eleven isolated rabbit hearts were arterially perfused with solution containing V_m-sensitive fluorescent dye (di-4-ANEPPS). The epicardium received shocks from symmetrical or asymmetrical electrodes to produce nominally uniform or nonuniform VGs. Extracellular electric field and ΔV_m produced by shocks in the absolute refractory period were measured with electrodes and a laser scanner and were simulated with a bidomain computer model that incorporated the anterior left ventricular epicardial fiber field. Measurements and simulations showed that fibers distorted extracellular voltages and influenced the ΔV_m. For both uniform and nonuniform shocks, ΔV_m depended primarily on second spatial derivatives of extracellular voltages, whereas the VGs played a smaller role. Thus, 1) fiber structure influences the extracellular electric field and the distribution of ΔV_m; 2) the ΔV_m depend on second spatial derivatives of extracellular voltage.

INTRODUCTION

The local extracellular voltage gradient (i.e., VG) has been used to measure shock thresholds for effects of cardiac electrical stimulation including cellular injury, myocardial excitation, reentry induction and defibrillation (Frazier et al., 1988, 1989; Ideker et al., 1991; Lepeschkin et al., 1978, 1980; Zhou et al., 1993). Such effects are thought to depend on the transmembrane voltage changes (ΔV_m) that are induced during the shock pulse. However, the VG may not determine the ΔV_m. One-dimensional continuous cable theory predicts that in the region beyond several space constants from a stimulation electrode there are no ΔV_m during a stimulation pulse, even though the VG is nonzero (Weidmann, 1970). To introduce ΔV_m in a continuous cable there may also need to be a local second spatial derivative of extracellular voltage or "activating function" (Rattay, 1989; Sobie et al., 1997). We have not found a publication in which the second spatial derivative of extracellular voltage during stimulation was measured in cardiac tissue. On the other hand, spatial variation of VG may not be required for ΔV_m to occur in the heart, because anatomical features of the heart that are not included in all models (e.g., structural discontinuities and fiber curvature) may introduce ΔV_m even where the VG is uniform (Krassowska et al., 1987; Plonsey and Barr, 1986; Trayanova et al., 1993).

The aim of this study was to examine the role of a spatial variation of VG in the ΔV_m in rabbit hearts. Electrical stimulation was performed to produce nominally uniform and nonuniform VGs in a region of the epicardium. Extracellular voltages and ΔV_m were measured using an array of recording electrodes and a laser scanner system with V_m-sensitive fluorescent dye. The voltages were also examined with a bidomain computer model that incorporated cardiac fiber orientations found in hearts.

Received for publication 28 December 1998 and in final form 27 May 1999.

Address reprint requests to Dr. Stephen Knisley, Department of Biomedical Engineering, University of Alabama at Birmingham, B122 Volker Hall, 1670 University Blvd., Birmingham, AL 35294-0019. Tel.: 205-975-4724; Fax: 205-975-4720; E-mail: sbk@crml.uab.edu.

0006-3495/99/09/1404/14 $2.00

MATERIALS AND METHODS

Experimental preparation

Hearts were removed from 11 pentobarbital-anesthetized New Zealand White rabbits in accordance with Institutional Animal Care and Use Committee guidelines. Hearts were arterially perfused as described (Knisley and Baynham, 1997). The perfusate contained (in mM) 129 NaCl, 4.5 KCl, 1.8 $CaCl_2$, 1.1 $MgCl_2$, 26 $NaHCO_3$, 1 Na_2HPO_4, 11 glucose, 0.04 g/L bovine serum albumin, bubbled with 95%/5% O_2/CO_2, at a pH of 7.3–7.4, an aortic pressure of 60–80 cm H_2O, and a temperature measured in the right ventricular cavity of 35–36°C. Diacetyl monoxime was added at a concentration of 15 mM to lessen motion effects in optical recordings (Li et al., 1985). This agent does not markedly alter the passive cardiac diffusion constant or stimulation-induced ΔV_m (Knisley, 1995; Knisley et al., 1993; Knisley and Hill, 1995).

Electrical stimulation

The heart was paced with a train of S1 pulses generated by a stimulus isolator (A365; World Precision Instruments, Sarasota, FL) to produce action potentials. The S1 had a 300-ms interval and 3-ms duration and was delivered from electrodes outside of the recording grid (bipolar) or near the center of the grid (unipolar).

Then a uniform or nonuniform shock (S2) of 5 ms duration was given at an S1–S2 interval of 80 ms, i.e., when cells were still refractory. This allowed the approximately passive response of the membrane during the pulse to be studied (Knisley et al., 1993). The S2 was generated with a bipolar power supply/amplifier (6827A; Hewlett Packard, Rockaway, NJ) and a photovoltaic relay (PVR1301; International Rectifier, El Segundo, CA). The S2 electrodes were parallel 4 × 32 mm stainless steel mesh (contact area ~1 cm^2) near the apex and base of the heart and a small Ag electrode above the recording grid (Fig. 1). The electric field produced with the two mesh electrodes in the myocardium was not completely uniform, because details of cardiac structure may influence the field. The distance between inside edges of mesh electrodes was 18 mm, so that recordings

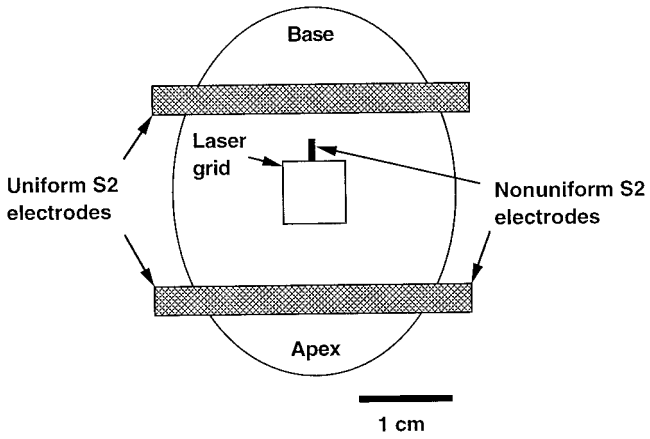

FIGURE 1 Sketch of S2 electrodes and laser recording grid on epicardium. Mesh stimulation electrodes (*cross-hatched rectangles*) were near base and apex of heart. Small S2 electrode (*filled bar*) was above the laser recording grid (*square*). Uniform S2 was applied from mesh electrodes. Nonuniform S2 was applied from the small electrode and the mesh electrode near the apex.

were obtained several space constants away from mesh electrode edges, where initial current redistribution between intracellular and extracellular spaces occurs (Weidmann, 1970). To produce a nonuniform S2 electric field, the small electrode was used in place of one of the mesh electrodes (Fig. 1).

Tests were performed with the electrode array on a 50-ml beaker filled with saline to verify the ability to generate and measure S2 electric fields in a homogeneous and isotropic medium and to help determine which S2 current strengths to use. Current strengths were sought for which uniform and nonuniform S2 produced a local VG of ~5–10 V/cm at the same location within the recording region. Such a VG is thought to produce effects in myocardium that are important for defibrillation (Knisley et al., 1992). The current strength for uniform S2 in hearts was ~200 mA or ~450 mA, and for nonuniform S2 it was ~50 mA. In two hearts, nonuniform S2 of ~120 mA was also tested. The VG depended on characteristics of the volume conductor as well as the current strength. With a given current strength, a noticeably larger VG occurred in a heart compared with the saline. Furthermore, VG in a heart decreased after electromechanically uncoupling with diacetyl monoxime, consistent with a rise in cavitary volume. Therefore extracellular shock voltages were directly recorded during optical recordings.

Electrical measurements

Metallic electrodes and leads to measure extracellular voltages produced by S2 can interfere with optical recordings by blocking excitation light or fluorescence. To overcome this, a limited measurement electrode array and careful alignment with optics were required. A single 6.4-mm linear array containing 16 Ag terminals was fabricated, with average terminal width 0.23 mm, terminal length 0.3 mm, and interterminal insulation space 0.12 mm. The terminals were cemented between edges of two coplanar glass microscope slides that contacted the heart (Knisley and Baynham, 1997). There was no conductive bath adjacent to the epicardium. The array was oriented approximately parallel or perpendicular to the apicobasal axis of the heart. Plate contact pressure was kept lower than perfusion pressure to avoid occlusion of epicardial vessels. The leads were arranged in a flat ribbon that was in a plane perpendicular to the glass and between laser beam paths for the laser measurement spots on either side of the terminals. Because the beam paths were approximately normal to the glass, the ribbon was also tilted 40° upward in its plane so that leads came out of the region of paths. The mirror that directed laser light to the heart was adjusted while the heart was viewed with a binocular magnifying loupe to ensure that terminals and leads did not block laser paths. Finally, the photomultiplier tube that collected the fluorescence was positioned immediately outside of laser paths and coplanar with the ribbon to ensure a straight-line path for fluorescence from each spot to the tube.

Each terminal in the array was connected to a 0.1 voltage divider that consisted of a 10^6 Ω resistor and a 111 kΩ resistor. The signals then passed through operational amplifiers (LT1014CN; Linear Technology Corporation, Milpitas, CA) in the unity gain configuration with an isolated battery-power supply.

Signals were unfiltered in initial trials and low-pass-filtered in later trials at a cutoff frequency (−3 dB) of 1.6 kHz to lessen wideband noise and not attenuate makes and breaks of S2. Signals were passed to a digitizer (MIO16; National Instruments Corporation, Austin, TX) and stored in a computer (Power Macintosh 7100-80; Apple Computer, Cupertino, CA). The digitizing range was ±10 V, which provided a measurement range before voltage dividers of ±100 V. To protect the digitizer in initial trials, each signal was also connected to a series of two oppositely biased zener diodes leading to the ground terminal of the amplifier and digitizer. The ground terminal was connected to a 2 cm^2 Ag/AgCl coil electrode mounted on a flexible arm and positioned on the opposite side of the heart.

In each trial, digital sampling was controlled by software (Labview; National Instruments Corporation). Data collection was initiated by a trigger pulse from the stimulation timer (A300; World Precision Instruments). Voltage at each electrode was sampled at a rate of 1 kHz. Measurements were reproducible when S2 was repeated under the same conditions.

In the first six hearts, shock voltages were measured only on the apicobasal axis. In five more hearts, shock voltages were measured in two dimensions, with the linear array perpendicular to the apicobasal axis and attached to a micromanipulator that allowed precise movement in the apicobasal direction. Epicardium, S1 and S2 electrodes, and the reference electrode were held stationary. Measurements for all 16 terminals were performed with the array at the basal side of the recording grid. Then the array was moved toward the apex (step size = 0.5 mm), and measurements were performed after each move. For all measurements, constancy of the shock current was verified with a series resistor, isolation amplifier, and digitizing oscilloscope. After a typical total movement of 6 mm (for a total of 208 measurements), the array was moved back to its starting position to reproduce the first measurements.

Fluorescence recording

Hearts were stained with 0.5–0.8 liters of perfusate containing 0.5 mg pyridinium, 4-(2-(6-(dibutylamino)-2-naphthalenyl)-1(3-sulfopropyl)-, hydroxide, inner salt (di-4-ANEPPS) (Molecular Probes, Eugene, OR) dissolved in 1 ml ethanol. Fluorescence signals that followed ΔV_m were measured with a laser scanner system using an argon laser with a wavelength of 514 nm (Hill and Courtney, 1987; Knisley, 1995). Acoustooptic deflectors steered the beam to scan 55 laser measurement spots with diameters of 100 μm in a 6 × 6 mm grid. Fluorescence was measured when the linear electrode array was near the center of the laser grid. Three rows or columns of spots were on one side of the array, and four were on the other side. Fluorescence emitted from the heart passed through a 590-nm long-pass filter and into a photomultiplier tube with a wide-band current-to-voltage amplifier. The fluorescence signal was filtered at 80 kHz to allow fast settling after the laser beam moved to a spot. The digitizing rate was 1 kHz for each spot (Knisley, 1995). Fluorescence collection was triggered by the stimulation timer.

Data analysis

For each terminal, the average extracellular voltage was measured in a 3-ms window during S2. Differences between averages for each pair of adjacent measurements were divided by the mean intermeasurement distance (0.426 mm in the direction parallel to the linear array and 0.5 mm perpendicular to the array) to obtain components of local VG. These

differences represented an average of the differences in tissue between the pair of measurements. Differences between pairs of adjacent local VG components in a given direction were divided by the mean intermeasurement distance to obtain the local spatial variation of VG. The Laplacian was the sum of spatial variations of VG in perpendicular directions.

The ΔV_m at each spot were determined as follows. The difference in fluorescence averages from a 3-ms window just before the S2 to a 3-ms window during S2 was determined. Each of the ΔV_m was this difference minus the difference in fluorescence averages at the same times relative to the action potential phase zero depolarization in a preceding action potential (control) that did not receive S2. The ΔV_m were expressed as a percentage of the amplitude of the action potential phase zero depolarization from the same recording (Knisley et al., 1993). To preserve the fast response of di-4-ANEPPS, recordings were not smoothed. Measurements were performed by a computer program and verified visually. Measurements were not affected by baseline shifts due to photobleaching. Contours of ΔV_m were generated with PV Wave (Snyder, 1978) or by hand.

Computer simulations

The bidomain model of excitable tissue is the best available model for the study of virtual electrodes and relationships between field-induced extracellular and V_m distributions (Henriquez, 1993). It has been shown (Sepulveda et al., 1989; Trayanova, 1996) to predict the electrically induced V_m distributions in hearts (Efimov et al., 1997; Knisley, 1995; Wikswo et al., 1995). We employed the bidomain model with a modified version (Skouibine et al., 1999) of the Beeler-Reuter-Drouhard-Roberge (BRDR) membrane kinetics (Beeler and Reuter, 1977; Drouhard and Roberge, 1982) to simulate the experiments in this study, in an attempt to elucidate the relationship between extracellular voltage and V_m distributions. The governing bidomain equations are

$$\nabla \cdot (\hat{\sigma}_e \cdot \nabla \Phi_e) = -\beta\left(I_{ion} + C_m \frac{\partial V_m}{\partial t}\right) - I_{stim} \quad (1)$$

$$\nabla \cdot (\hat{\sigma}_i \cdot \nabla \Phi_i) = \beta\left(I_{ion} + C_m \frac{\partial V_m}{\partial t}\right) \quad (2)$$

where $\Phi_{e,i}$ are the extra- and intracellular voltages, and $V_m \equiv \Phi_i - \Phi_e$. β is the surface area-to-volume ratio. I_{ion} is the ionic current determined by the modified BRDR membrane kinetics. C_m is the membrane capacitance, and I_{stim} is the stimulus current, applied extracellularly. Finally, $\hat{\sigma}_{e,i}$ are the global conductivity tensors that depend on the local fiber direction and the conductivities in the directions longitudinal and transverse to fibers for the extra- and intracellular spaces:

$$\hat{\sigma}_{e,i} = (d^T \cdot d) \cdot (g_{l;e,i} - g_{t;e,i}) + \hat{I} \cdot g_{t;e,i} \quad (3)$$

(Colli-Franzone and Guerri, 1993), where $d^T \cdot d$ is the outer product of the unit vector parallel to the local fiber direction and its transpose; $\hat{I}$ is the identity matrix; and g_l and g_t are the local conductivities in the direction parallel and transverse to fibers in the extra- and intracellular spaces. In an attempt to mimic the experimental conditions, we used sealed-end boundary conditions:

$$\hat{n} \cdot (\hat{\sigma}_e \cdot \nabla \Phi_e) = 0 \quad (4)$$

$$\hat{n} \cdot (\hat{\sigma}_i \cdot \nabla \Phi_i) = 0 \quad (5)$$

where $\hat{n}$ is the unit vector normal to the tissue boundaries.

The equations were discretized using a finite difference scheme that is second-order accurate in space and first-order accurate in time. The boundary conditions were discretized on a layer of nodes at which Eqs. 4 and 5 hold. Second-order accuracy was maintained at the boundaries by using a three-point backward or forward difference discretization of first derivatives.

A direct method was used to solve the differential-algebraic equations that result from the discretization of Eqs. 1 and 2 and 4 and 5. Because tissue properties were constant throughout the simulations, a lower-triangular, diagonal, upper-triangular (LDU) decomposition was carried out only once. For each time step, the right-hand side vector was calculated using the modified BRDR membrane kinetics and the intracellular and extracellular voltages (and hence V_m) found in the previous time step. Using the updated right-hand side, the calculated LDU decomposition was then used to efficiently solve the large system of algebraic equations for the intracellular and extracellular voltages. By using this solution scheme, it was possible to inject current at a given location in the tissue and remove current by simply grounding (i.e., setting the extracellular voltage to zero) another region in the tissue.

The experimental protocols were duplicated as closely as possible without compromising the computational feasibility of the simulations. Because of these concerns and the fact that no accurate measurements could readily be made through the ventricular wall in the experimental portion of the study, a two-dimensional geometry was used for the model studies. The fiber field was taken from one heart and contained features of the epicardial fiber structure near the anterior left ventricular recording region that were common to all six hearts examined with the blue dye. Fiber directions more than ~10 space constants away from the recording region, which were too far away to affect our results, were estimated by extrapolation. Along with Clerc's local conductivity measurements (Clerc, 1976), the fiber field was used to calculate the global conductivity tensors that appear in the bidomain equations, using Eq. 3.

The size of the tissue in the simulations was 2.48 × 2.64 cm. The discretization step size was 200 μm in both the x and y directions, and the time step was 10 μs. In all figures that show model results, a 6 × 6 mm central area of the model is displayed that corresponds to the recording region near the center of the heart in the experimental protocol. A 4 × 24.8 mm S2 ground electrode was located at the bottom of the tissue model. An S1 pulse was delivered via an electrode above the recording region to elicit an action potential. A 5-ms S2 was then delivered 80 ms after the S1 either via a small electrode just above the recording region to establish a nonuniform extracellular S2 electric field or via a 4 × 24.8 mm S2 electrode at the top of the tissue to establish a uniform field. Within the recording region, the extracellular VG produced by the S2 ranged from 5.9 to 36.3 V/cm for the nonuniform S2 and from 11.1 to 14.1 V/cm for the uniform S2.

RESULTS

Nonuniform field stimulation

Fig. 2 shows the effect of nonuniform S2 on V_m at individual recordings (Fig. 2 *A*) and the entire recording grid (Fig. 2 *B*). The upper left quadrant of the grid underwent positive ΔV_m, and the upper right quadrant underwent negative ΔV_m. In the seven hearts in which ΔV_m were measured on the anterior left ventricle, the mean ΔV_m (expressed as a percentage of action potential amplitude) in upper left and right quadrants were 13.5 ± 12.9 and −17.6 ± 17.8 when the small electrode was the cathode ($p = 0.006$, for left versus right, t-test) and −14.3 ± 14.7 and 7.1 ± 13.8 when the small electrode was the anode ($p = 0.03$).

Fig. 3 shows the distributions of the extracellular voltages produced by nonuniform S2. Variations in the voltage gradient existed in two dimensions. The fall of the extracellular voltage with distance in Fig. 3 was not purely symmetrical about the apicobasal axis. Instead, voltages were larger in regions closer to the left lateral heart (i.e., right side of graph). In the four hearts in which extracellular voltages were mapped in two dimensions during nonuniform S2 on

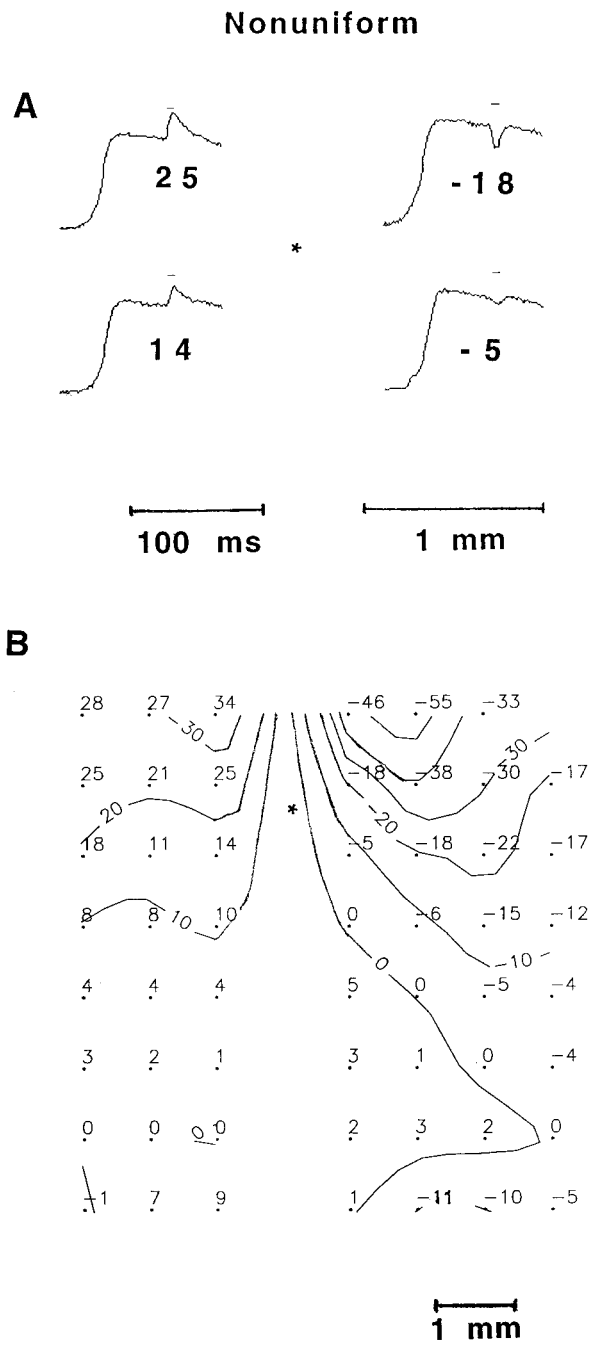

FIGURE 2 Effect of nonuniform S2 on the transmembrane voltage (V_m). The small S2 electrode just above the recording grid was cathodal, and the mesh electrode near the apex was anodal. (*A*) Fluorescence recordings from neighboring laser spots near the boundary (*) between regions, in which V_m changes had opposite signs (*asterisk*). The local voltage gradient on the apicobasal (vertical) axis was 7.4 V/cm. Each recording shows the phase zero depolarization produced by S1 stimulation and the V_m change produced by S2 given during the plateau phase of the action potential. The timing of the S2 is shown by the horizontal bar above each recording. Signs and magnitudes of V_m change as a percentage of the action potential amplitude are shown below plateau portions of each recording. (*B*) Measurements and contour plot of the distribution of V_m changes at all laser spots. The S2 strength was 44 mA.

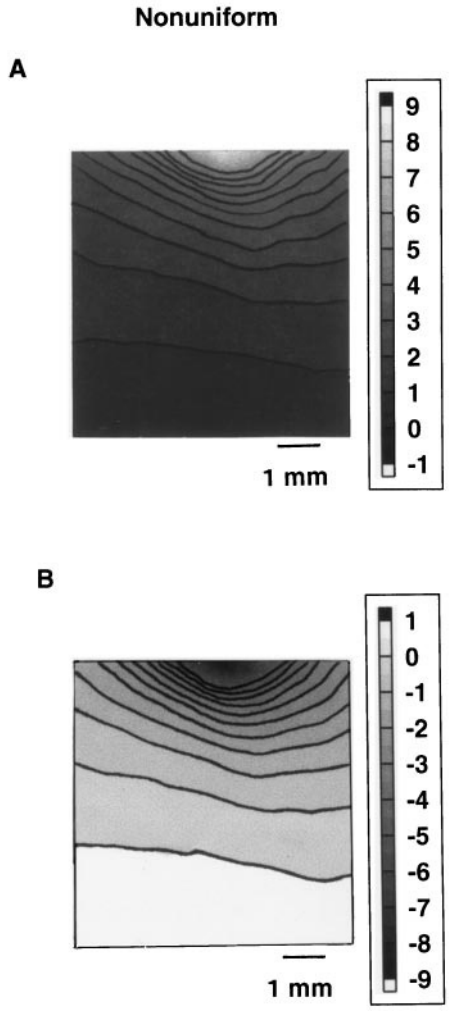

FIGURE 3 Extracellular voltage distribution (V) in recording grid during nonuniform S2. In *A*, the small S2 electrode just above the recording grid was anodal, and the mesh electrode near apex (below grid) was cathodal. In *B*, the polarity was reversed (i.e., polarity as in Fig. 2). The S2 strength was 55 mA.

the anterior left ventricle, the most apical point of the extracellular isovoltage contour at midheight in the recording region was 1.4 ± 0.7 mm to the right of center (p = 0.025, t-test). If fibers had no effect or were absent (e.g., in an isotropic medium), we would expect this point at the center.

We evaluated approximate fiber direction in the recording region of four hearts from activation times by using the fact that action potential propagation near the origin of excitation is faster along fibers versus across fibers (Spach and Barr, 1975; Roberts and Scher, 1982; Knisley, 1995). Fig. 4 shows measurements of S1-induced activation times. The S1 electrode was near the center of the recording grid. On the anterior left ventricle of three hearts, the fast axis was significantly tilted from the upper left to lower right at an angle of −19.2 ± 3.8° (p = 0.013, t-test).

We further studied fiber direction by direct visual examination of six hearts after the completion of the experiments

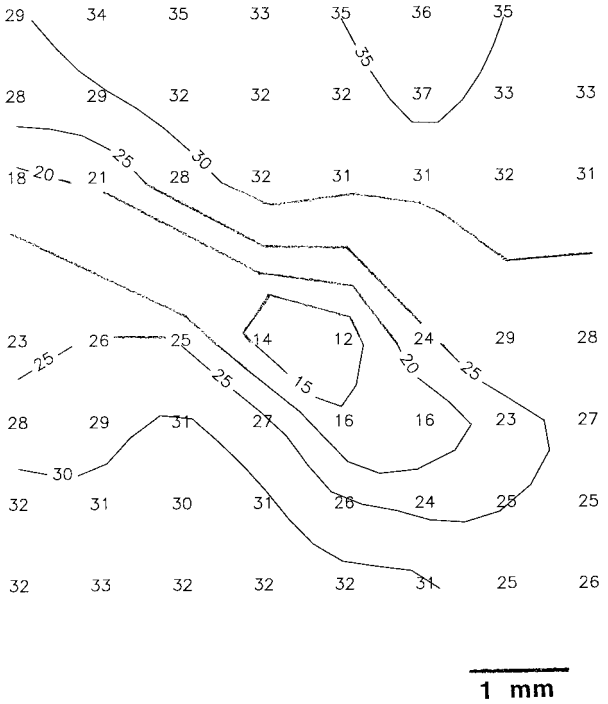

FIGURE 4 Contour plot of activation times (ms) after S1 stimulation in diastole from an electrode within the recording grid. Contour lines are drawn from 15 to 35 ms in 5-ms increments.

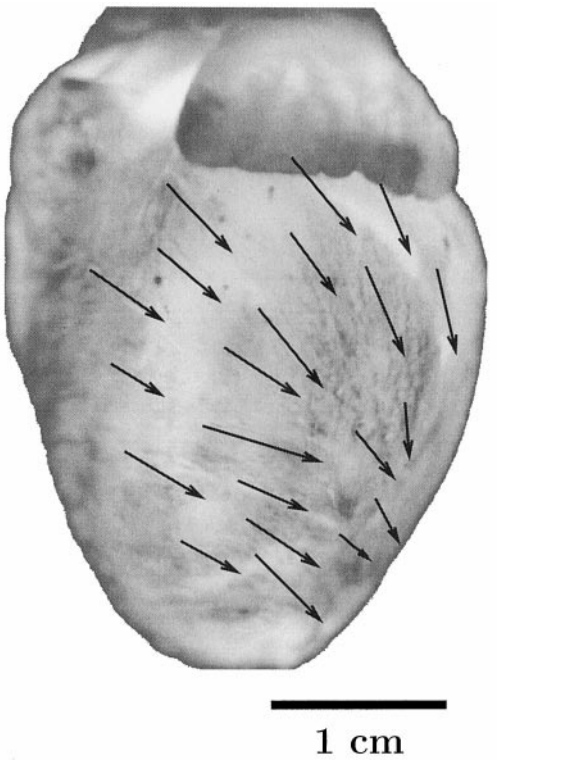

FIGURE 5 Anterior view of rabbit heart, showing epicardial surface. The fluorescence recording grid was in the approximate center. Linear marks indicate the fiber field that was used in the bidomain computer model. Fibers became more horizontal in epicardium toward the apex, and more vertical in the left lateral epicardium.

and fixation of the hearts with formalin (Nielsen et al., 1991). Hearts were held with approximately coaxial needles that penetrated the heart from the base and apex to minimize epicardial distortion. The direction of minute epicardial grooves was taken as the epicardial fiber direction (LeGrice et al., 1995). Fig. 5 shows the anterior of a rabbit heart observed after staining with Evans Blue dye and transilluminating. The average fiber direction in the recording grid (center) was from the upper left to lower right.

The visual examinations also indicated that fibers curved in the hearts. Fiber curvature has been predicted to affect the ΔV_m (Trayanova, 1993; Trayanova and Skouibine, 1998). In all six hearts studied with blue dye, fibers became more horizontal in epicardium toward the left ventricular anterioapical region and more vertical toward the left lateral region.

We hypothesized that the ΔV_m in Fig. 2 result from a nonuniform electric field that is not simply determined by electrode geometry, but instead is the field produced with the small electrode modulated by the fiber orientation on the epicardium. To test this, we performed computer simulations that incorporated the S2 electrode geometry and epicardial fiber structure. The structure is shown by the linear marks in Fig. 5. The structure near the anterior recording region is consistent with a recent detailed study of rabbit ventricular anatomy by Vetter and McCulloch (1998). Fig. 6 shows that the simulated ΔV_m were positive in the region that corresponded to the upper left quadrant of the recording grid and negative in the region that corresponded to the upper right quadrant. The model results agreed with the measurements of ΔV_m in the upper left and right quadrants. For both quadrants and both electrode polarities combined, the sign test rejected the null hypothesis that the probability of agreement with the model was 0.5 ($p = 0.0002$, $n = 28$) (Mendenhall et al., 1986). Thus the two-dimensional bidomain model incorporating appropriate geometry of the S2 electrode and epicardial fibers is sufficient to explain signs of ΔV_m during nonuniform S2.

Furthermore, the bidomain model demonstrated that the extracellular electric field produced with the small S2 electrode was modulated by fiber structure. Fig. 7 shows that extracellular voltage contours tilted toward the right side of the graph, as they did in hearts (Fig. 3).

Uniform field stimulation

Fig. 8 shows ΔV_m during uniform S2 in a rabbit heart and in the bidomain model. In the heart (Fig. 8 *A*), negative ΔV_m occurred in the lower left quadrant and upper half of the grid, and positive ΔV_m occurred in the upper left and lower right. Magnitudes of ΔV_m were frequently as large in lower quadrants as in upper quadrants. The model (Fig. 8 *B*) produced ΔV_m that agree with measurements shown in Fig. 8 *A*.

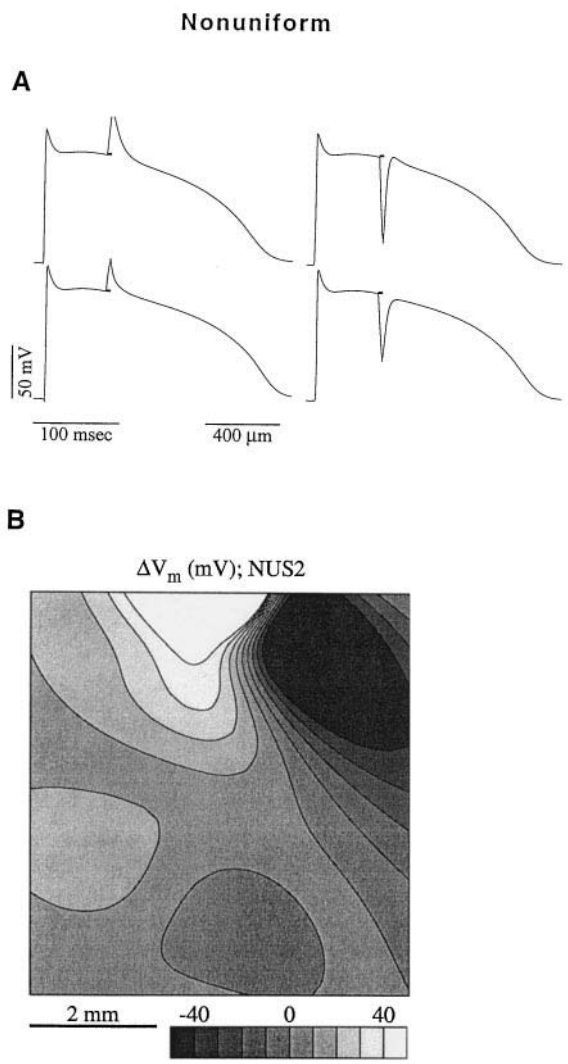

FIGURE 6 Results of the bidomain model, showing the effect of nonuniform S2 on transmembrane voltage (V_m). The timing of the S2 is shown by the horizontal bar at the plateau level of each simulated action potential. The small S2 electrode located just above the recording grid was cathodal. (*A*) Computed V_m at sites that correspond to the four recordings in Fig. 2 *A*. (*B*) The distribution of the V_m change in the recording grid during S2, which corresponds to Fig. 2 *B*. The S2 strength was 44 mA.

The ΔV_m during uniform S2 varied among hearts. For example, in one heart with the electrode nearer the apex as the cathode, no ΔV_m that had a positive sign occurred at any laser recording spot, whereas the ΔV_m were negative at 54 spots and zero at one spot, and in another heart the ΔV_m had a positive sign at 15 spots and a negative sign at 36 spots, and were zero at four spots. The sign of ΔV_m frequently was constant for a group of adjacent spots. In no case was an individual spot found that had a given sign of ΔV_m and was surrounded by neighboring spots with the opposite sign of ΔV_m.

Fig. 9 shows the distribution of extracellular voltage during uniform S2 in a heart and in the model. The gradient of the S2 voltage was approximately constant. Despite the uniformity of the applied electric field, extracellular voltage

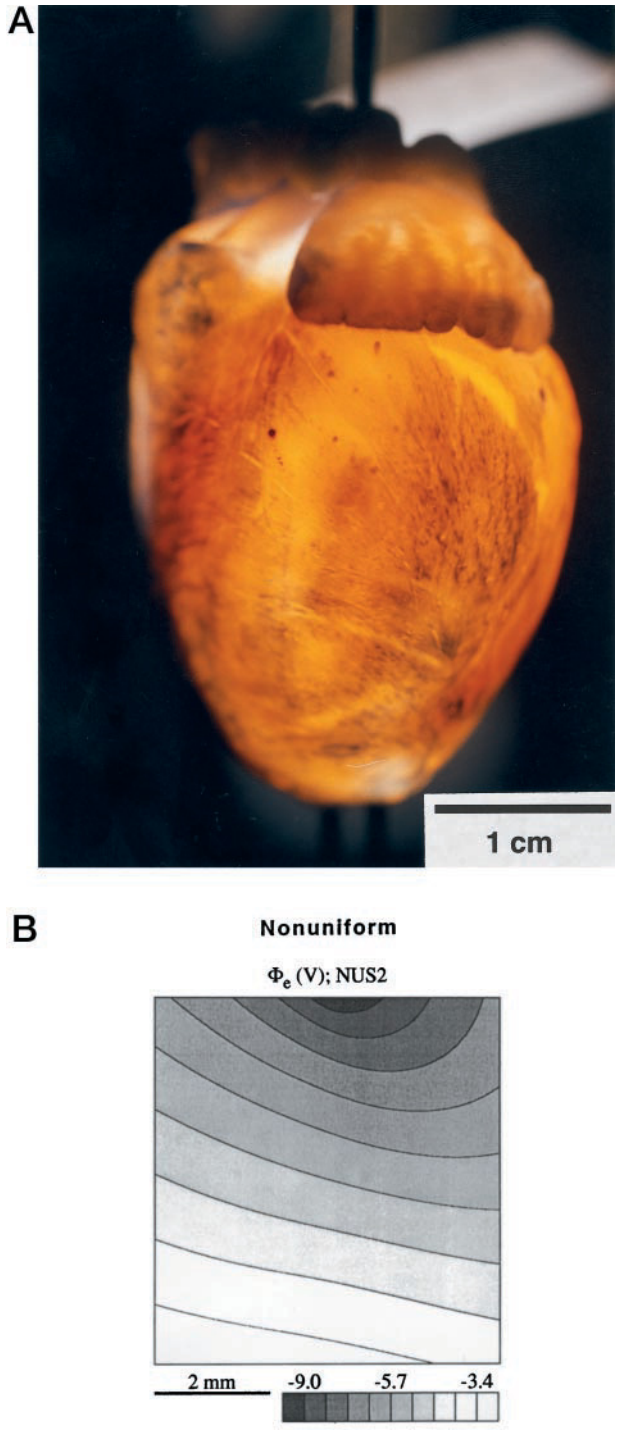

FIGURE 7 Tilt of epicardial fibers and extracellular voltages during nonuniform S2. (*A*) Evans blue-stained heart, showing tilt of anterior left ventricular fibers from upper left to lower right of the Figure. (*B*) Results of the bidomain model, showing the distribution of extracellular voltages produced by the same nonuniform S2 as in Fig. 6. Extracellular voltage contours are tilted because of fiber orientation. The small S2 electrode just above the recording grid was cathodal.

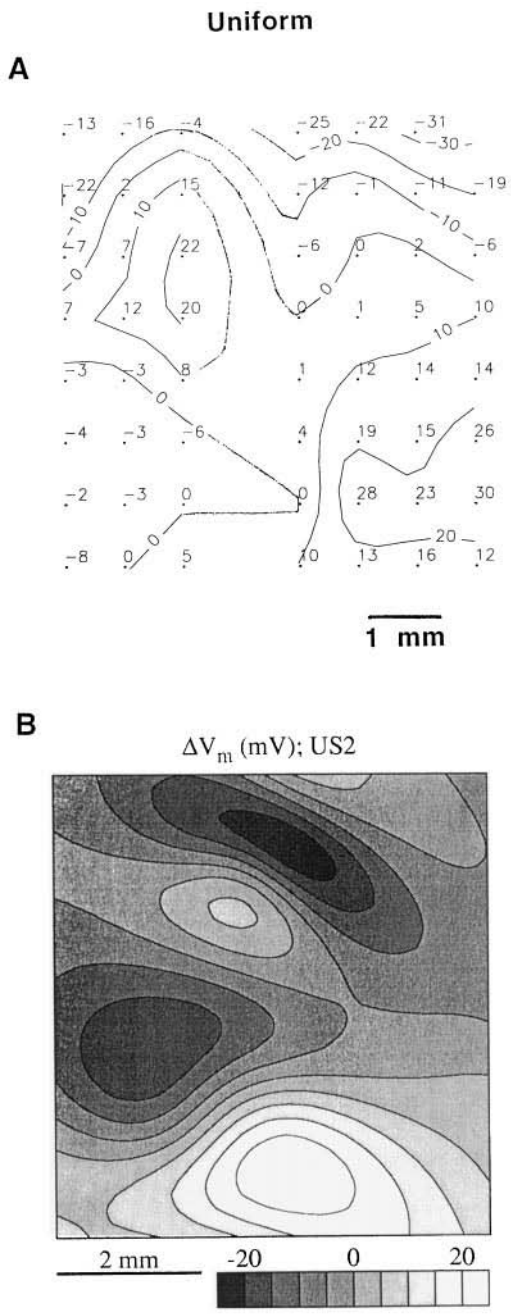

FIGURE 8 The effect of uniform S2 on transmembrane voltage (V_m). (*A*) Measurements from a rabbit heart (% of action potential amplitude). (*B*) Bidomain model results. The S2 electrode near the base of the heart or the top of the model was cathodal. The S2 strength was 312 mA.

contour lines were not horizontal, as evident from the tilt of isovoltage lines in the model (Fig. 9 *C*). Thus even with uniform S2, fiber orientation distorts extracellular voltages in the model, indicating that the extracellular field depends upon both the applied electric field and fiber structure. Tilt was smaller in hearts, which may be due to fiber rotation in deeper layers. In four hearts during uniform S2 on the anterior left ventricle, the isovoltage contours in the approximate center of the recording region were at an angle of $-1.3 \pm 3.7°$ ($p = 0.5$, *t*-test).

Origin of the transmembrane voltage changes

The model of shock-induced ΔV_m demonstrates close agreement with experimental results. This allows us to use the model to understand the factors that contribute to ΔV_m during uniform and nonuniform S2. The relationship between transmembrane and extracellular voltages in the first bidomain equation (Eq. 1) can be represented as follows:

$$-\beta\left(I_{ion} + C_m \frac{\partial V_m}{\partial t}\right) = g^e_{xx}\frac{\partial^2\Phi_e}{\partial x^2} + g^e_{xy}\frac{\partial^2\Phi_e}{\partial x\partial y} + g^e_{yx}\frac{\partial^2\Phi_e}{\partial x\partial y} + g^e_{yy}\frac{\partial^2\Phi_e}{\partial y^2} + \frac{\partial g^e_{xx}}{\partial x}\frac{\partial\Phi_e}{\partial x} + \frac{\partial g^e_{xy}}{\partial x}\frac{\partial\Phi_e}{\partial y} + \frac{\partial g^e_{yx}}{\partial y}\frac{\partial\Phi_e}{\partial x} + \frac{\partial g^e_{yy}}{\partial y}\frac{\partial\Phi_e}{\partial y} \quad (6)$$

The left hand-side of this equation is $-\beta I_m$, where I_m is the total transmembrane current density. In the passive case, which approximates the membrane response during the plateau of an action potential, the ΔV_m at a given time during S2 are proportional to I_m. The right-hand side of the above equation is then proportional to $-\Delta V_m$. Comparison between ΔV_m shown in Figs. 6 *B* and 8 *B*, and the right-hand side of Eq. 6 shown in Figs. 10 *C* and 11 *C*, respectively, clearly demonstrates this proportionality with a negative sign.

Examining Eq. 6, one sees that the relationship between ΔV_m (with a negative sign) and Φ_e can be considered as consisting of two parts. The first part (the first four terms on the right) relates the shock-induced ΔV_m to the second spatial derivatives of extracellular voltage. The coefficients of proportionality are the tissue conductivities. The second part of this relationship (i.e., the second group of four terms on the right) involves the first derivatives of the extracellular voltage (the components of the extracellular VG). The coefficients of proportionality are the derivatives of the global conductivities, which are nonzero when the fibers curve in space.

Thus, from Eq. 6 one can conclude that in the case in which the fibers were straight, the relationship is then reduced to only the first part, i.e., ΔV_m are related to the derivatives of extracellular VG. Alternatively, if the extracellular voltage gradient is uniform, then the first part of the relationship vanishes, leaving V_m as a function of the components of the extracellular VG. However, neither of these two conditions is fulfilled in the real case. In the heart, fiber orientation changes and the extracellular voltages are distorted by fibers, even if the applied field is uniform. This behavior of the extracellular voltage is clearly observed in Fig. 9 *C*. Thus, both groups of terms contribute to ΔV_m; it is their relative magnitude that is altered when the S2 is switched from uniform to nonuniform, as demonstrated below.

Figs. 10 and 11 display maps of the sum of the first group of terms, the sum of the second group of terms, and the sum of all terms in Eq. 6 for nonuniform and uniform S2 stim-

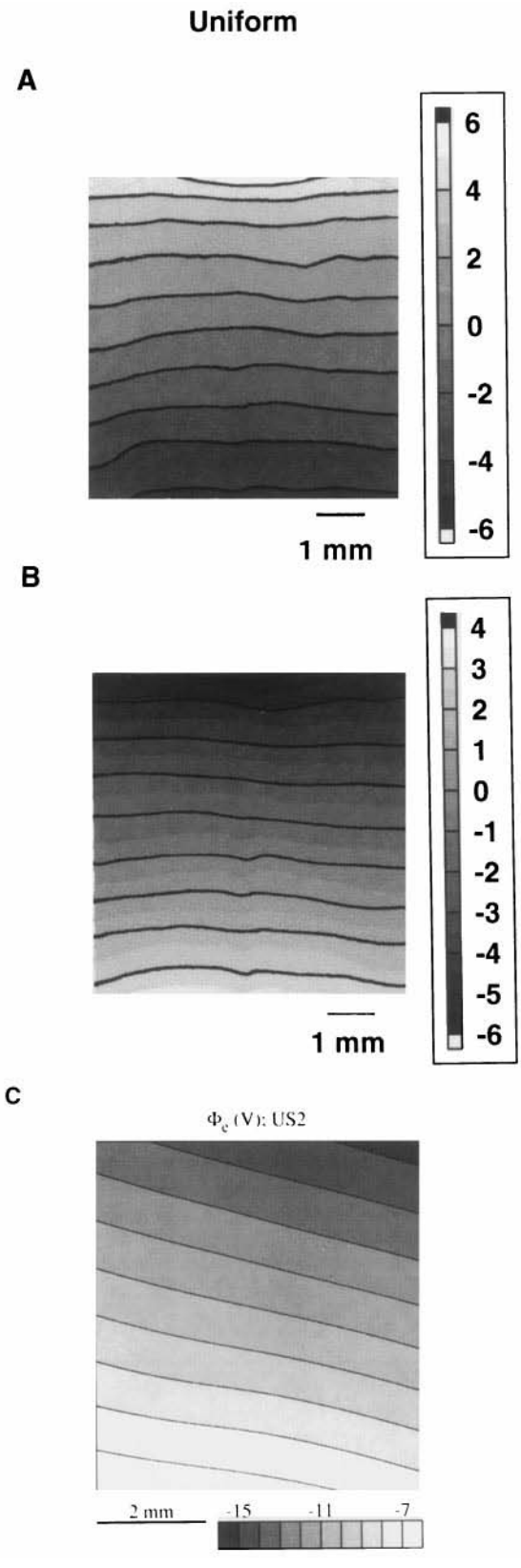

FIGURE 9 Maps of extracellular voltage during uniform S2. (*A* and *B*) Measurements (*V*) from a rabbit heart for both S2 polarities. (*C*) Bidomain model results for the S2 polarity of *B*. The S2 strength was 220 mA in the heart and 312 mA in the model.

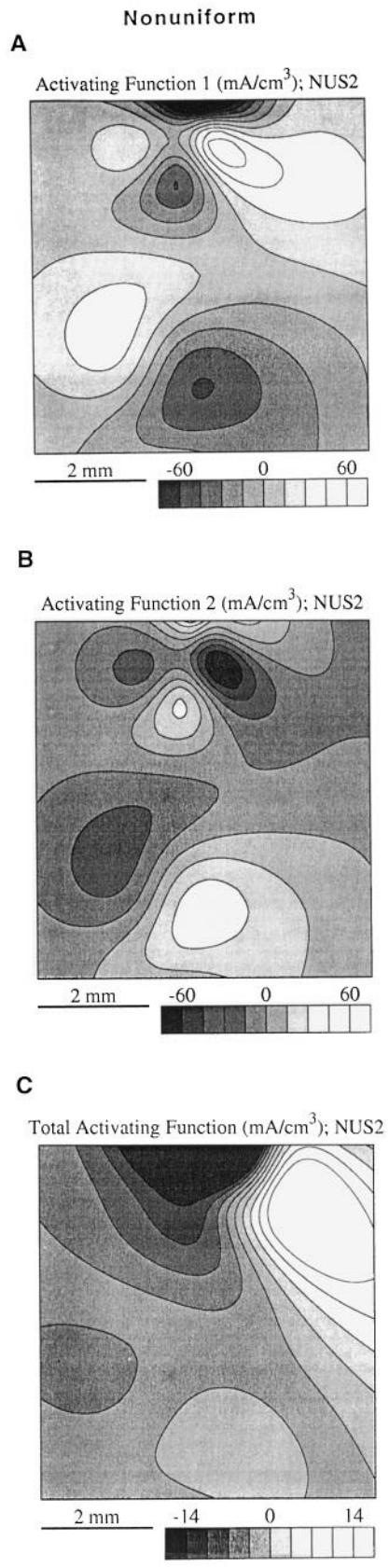

FIGURE 10 Maps of "activating functions" for nonuniform S2 in bidomain model. (*A*) "Activating function 1," i.e., the first group of four terms in Eq. 6. (*B*) "Activating function 2," i.e., second groups of terms in Eq. 6. (*C*) "Total activating function," i.e., right-hand side of Eq. 6.

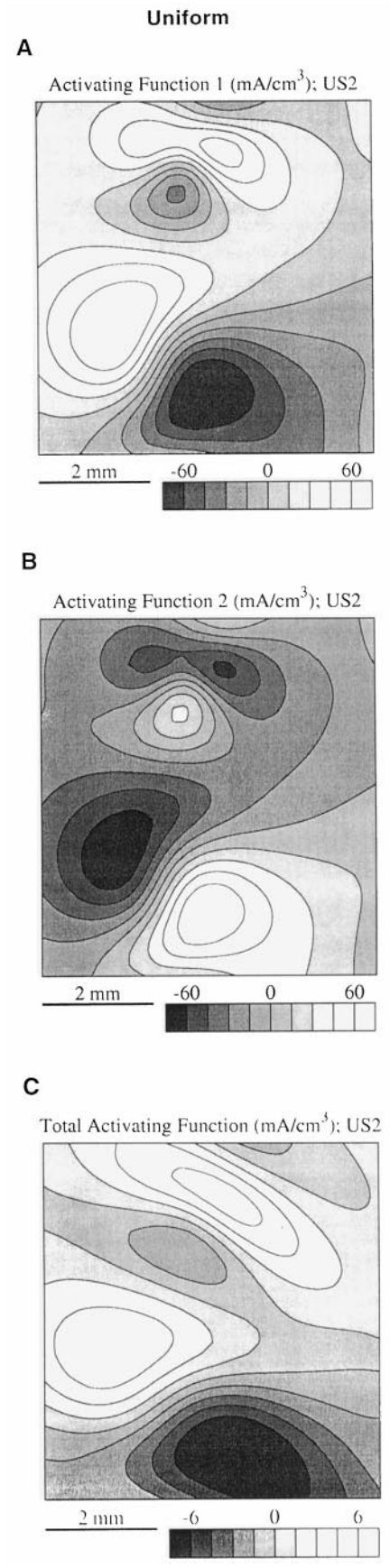

FIGURE 11 Maps of "activating functions" for uniform S2 in the bidomain model. The panels are defined as in Fig. 10.

ulation. These are called "activating function 1," "activating function 2," and "total activating function," respectively, following terminology by Rattay (1989) and Sobie et al. (1997). Thus, it is expected that Figs. 10 *C* and 11 *C* will provide the pattern of shock-induced ΔV_m, as seen in Figs. 6 and 8, but with an opposite sign, in accordance with Eq. 6. Indeed, the similarity is clearly evident upon visual inspection of these figures. In the case of a nonuniform S2 (Fig. 10), the first and second groups of terms have similar patterns, but the deflections are in opposite directions. When they are added, the deflections partly cancel each other. The sum of the two plots ("total activating function") has a range of magnitudes four times smaller than that of the original plots.

Therefore, when the applied shock is nonuniform, both groups of terms in Eq. 6, i.e., terms that contain second derivatives of extracellular voltage and terms that contain VGs, contribute to the pattern in Fig. 10 *C*. The terms for the second derivatives make a larger contribution because deflections in Fig. 10 *C* often retain the shape and sign of those in Fig. 10 *A*, which is most notable near the top, where deflections are large. For all computed points in Fig. 10, the RMS difference between Fig. 10, *A* and *C*, was 20.2 mA/cm^3, whereas the RMS difference between Fig. 10, *B* and *C*, was 55.4 mA/cm^3. The smaller difference between Fig. 10, *A* and *C*, indicates that "activating function 1" contributes more to the "total activating function" than does "activating function 2."

For the case of a uniform S2, Fig. 11, *A* and *B*, shows "activating function" maps with deflections in opposite directions that largely cancel each other. The pattern of the "total activating function" (Fig. 11 *C*) retained the shape and sign of the deflections in Fig. 11 *A*. However, unlike the nonuniform S2, contributions of second derivatives of extracellular voltage were only slightly larger than contributions of voltage gradients. This is evident from the range of the "total activating function" (Fig. 11 *C*), which was 10 times smaller than the ranges in the original plots. The RMS difference between Fig. 11, *A* and *C*, was 31.5 mA/cm^3, whereas the RMS difference between Fig. 11, *B* and *C*, was 34.1 mA/cm^3, indicating a slightly greater contribution by "activating function 1."

As a final verification that model and experiment agree, and thus considerations made above apply to the stimulation of real myocardium, a comparison was made between the calculated and experimentally recorded Laplacians of extracellular voltage (or, equivalently, the first four terms in Eq. 6, assuming the conductivities are unity). Fig. 12 shows the Laplacian maps during nonuniform S2 for the S2 polarity in which the small electrode above the recording grid was the cathode. Experimental measurements and contours of ΔV_m are overlaid upon the experimental Laplacian map from the same heart (Fig. 12 *A*). In both experiment and model, the top region of the graph contained a negative Laplacian on the left side and a positive Laplacian on the right side. When the S2 polarity was reversed (not shown), the signs of the Laplacians on the left and right sides reversed. In the four hearts in which extracellular voltages were measured in two dimensions on the anterior left ventricle, when the small

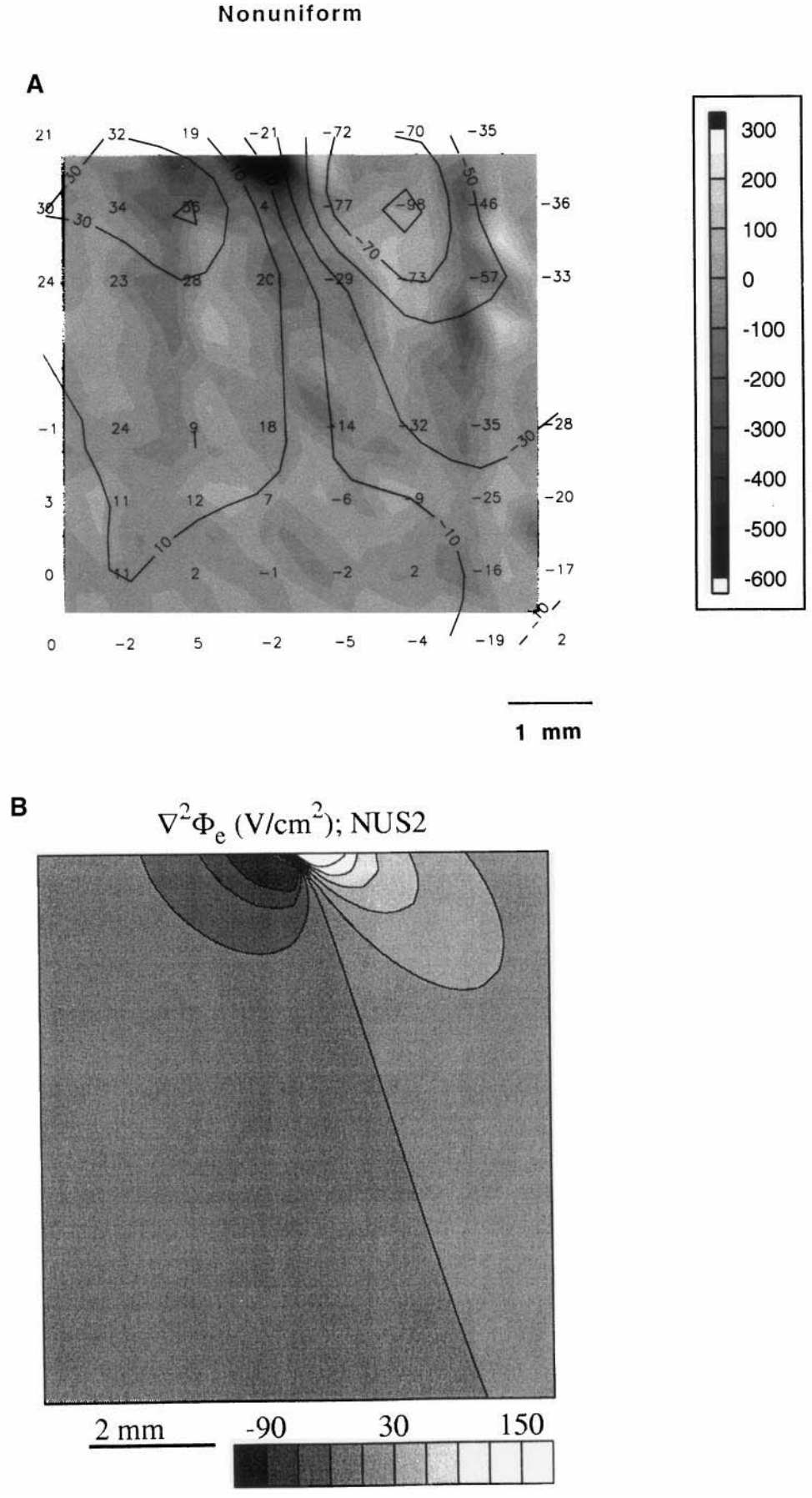

FIGURE 12 Maps of Laplacian of extracellular voltage during nonuniform S2. (*A*) Epicardial measurements (V/cm^2) from a rabbit heart. Transmembrane voltage changes (*numbers and contour lines*) are overlaid on a gray-scale Laplacian for the same heart. (*B*) Bidomain model results. The S2 strength was 56 mA in the heart and 44 mA in the model.

electrode was the cathode, the Laplacian was more negative on the top left compared with the top right. When the small electrode was the anode, the Laplacian was more negative on the top right compared with the top left, which again agreed with the model. For the two electrode polarities combined, the sign test rejected the null hypothesis that the probability of agreement with the model was 0.5 ($p = 0.008$, $n = 8$).

DISCUSSION

This study examined the V_m and extracellular voltage changes induced in rabbit hearts during an electric shock for both uniform and nonuniform applied fields. A computer model representing the experimental preparation was also assembled and used to calculate the corresponding V_m and extracellular voltages. The model, which demonstrated excellent agreement with the experiment, was further used to relate ΔV_m to extracellular voltages and their derivatives and thus aid in understanding the factors responsible for ΔV_m during the shock.

Distributions of transmembrane and extracellular voltage changes during S2

The distribution of ΔV_m found in the laser recording grid during the nonuniform S2 had features that would be expected in regions surrounding the small stimulation electrode. Taking into account the specific fiber orientation in the region of recording (Figs. 4 and 5), a portion of the familiar "dog-bone" pattern is observed (Figs. 2 and 6). Such a pattern has been documented in both computer simulation (Sepulveda et al., 1989; Trayanova et al., 1998) and experimental studies (Knisley et al., 1994, 1995; Neunlist and Tung, 1995; Wikswo et al., 1995). Indeed, because the average fiber orientation is parallel to a line from upper left to lower right, the upper right portion of the plot for nonuniform S2 in Fig. 2 *B* is away from the small stimulation electrode in the direction parallel to the fibers. This is the direction along which the sign of ΔV_m reverses away from a point electrode, producing negative ΔV_m during cathodal stimulation. Moreover, the positive ΔV_m in the upper left portion of the plot are expected because the sign of ΔV_m does not reverse away from the electrode in the direction perpendicular to fibers. The fact that the small electrode used to produce nonuniform S2 was not a single point does not prevent reversal of the sign of ΔV_m away from the electrode in the direction along fibers, which is evident from studies of line stimulation (Knisley and Baynham, 1997; Knisley et al., 1994).

A uniform S2 resulted in a rather different distribution of ΔV_m. Regions of positive and negative ΔV_m could be found throughout the recording grid of our model. There are few published data to compare, because ΔV_m during S2 delivered from symmetrical electrodes on hearts were reported at only one or a few spots, and the uniformity of the S2 electric field was not measured (Holley and Knisley, 1997; Zhou et al., 1995). Only a handful of model studies (Sobie et al., 1997; Entcheva et al., 1998, 1999; Trayanova et al., 1993, 1998) document the involvement of fiber curvature in the ΔV_m under conditions of electric stimulation. Most of these models employed stylized fiber fields. Here we incorporate a realistic fiber orientation found in rabbit heart. Furthermore, our preliminary simulation in which fibers were straighter than those of the heart used in Fig. 8 produced less agreement with the experiment, which supports a role of fiber curvature in the generation of ΔV_m.

The extracellular voltage distributions are strictly nonuniform for both uniform and nonuniform S2, with the highest nonuniformity near the small electrode for nonuniform S2 (Figs. 3, 7, and 9). These distributions demonstrate an important point: even for a uniform S2, isovoltage lines do not coincide with a uniform applied field. This is because the fiber orientation in the myocardium distorts the electric field. Thus the extracellular shock voltage that actually occurs in the myocardium is distinctly different from the applied shock field, i.e., the field that would be produced in a homogeneous isotropic volume conductor if fibers were neglected (Rattay, 1989).

Does voltage gradient determine transmembrane voltage changes?

Numerous investigations have quantified electric stimulation efficacy in the tissue by the local extracellular VG during the shock (Ideker et al., 1991; Lepeschkin et al., 1978, 1980). However, the VG may not determine the ΔV_m, which is strongly indicated by ΔV_m in different parts of the recording grid. For nonuniform S2, positive ΔV_m occur on the left side of the map in Fig. 2, and negative ΔV_m occur on the right. This is true even for spots near the main apicobasal axis (Fig. 2 *A*), where extracellular VG is similar (Fig. 3). Moreover, the uniform S2 in Fig. 8 produced heterogeneous ΔV_m, even though the VG did not vary greatly (Fig. 9). If VG alone determined the ΔV_m, we would expect the VG to be very different among the regions where ΔV_m have opposite signs.

In this study we demonstrate that the ΔV_m in the recording region are predominantly due to second spatial derivatives of extracellular voltage (Fig. 10). Although this is most clearly seen for the nonuniform S2, even in the case of a uniform S2 where the extracellular VG was expected to dominate (Sobie et al., 1997; Trayanova et al., 1998), we still observe quantitative prevalence of the terms containing the second spatial derivatives of extracellular voltage (Fig. 11). Because terms containing the VG in Eq. 6 depend upon spatial changes in conductivity, future studies may reveal whether the terms become larger if fiber orientation changes more rapidly or if cells become electrically uncoupled, as occurs in ischemia. Our finding that fiber structure alters the electric field suggests that contributions of second spatial

derivatives of extracellular voltage may also become larger with curvature or cellular uncoupling.

To reach our conclusions, we used our model of electric stimulation that incorporated the relationship between the transmembrane and extracellular voltage changes induced by the shock. This relationship is governed by Eq. 6. This, however, is not the only way the relationship between V_m and Φ_e could be expressed mathematically in the bidomain model. Alternative equations are offered by Sobie et al. (1997) and Trayanova et al. (1998). All of these equations represent generalizations of the "activating function" theory of Rattay (1989). The equations derived by Sobie et al. (1997) and Trayanova et al. (1998) incorporate either the intracellular conductivities (Sobie et al., 1997) or combinations of intra- and extracellular conductivities (Trayanova et al., 1998), as well as additional terms that involve the derivatives of V_m. Although examination of these equations ultimately may result in the same general conclusions regarding the relationship between V_m, the derivatives of Φ_e, and fiber orientation (Sobie et al., 1997; Trayanova et al., 1998), we chose Eq. 6 for our numerical analysis because it is straightforward and relatively simple in relating V_m and Φ_e. When the different terms of this equation were numerically calculated for the particular fiber structure of the experimental preparation, quantitative conclusions regarding the contributions of extracellular VG and its derivatives to ΔV_m could be obtained.

The finding that the extracellular VG does not determine ΔV_m during the shock has some support in other studies of cardiac stimulation. The ΔV_m during a unipolar stimulation pulse in the heart have opposite signs at different sites away from the electrode in the direction parallel to the cardiac fibers (Knisley et al., 1994, 1995; Neunlist and Tung, 1994, 1995; Wikswo et al., 1995), although the sign of the extracellular VG does not reverse among the sites (Sepulveda et al., 1989). Such results were predicted by two- or three-dimensional theory of myocardium with realistic resistance anisotropy (Roth and Wikswo, 1994; Sepulveda et al., 1989; Entcheva et al., 1998, 1999; Trayanova et al., 1998). Furthermore, studies of electric field stimulation of isolated cardiac myocytes showed that excitation depends not only on VG but also on myocyte orientation with respect to the VG (Tung et al., 1991). The ΔV_m at ends of myocytes aligned with the electric field have opposite signs when the sign of the VG is constant and depend on myocyte size (Knisley et al., 1993). Irreversible injury is a function of myocyte orientation (Knisley and Grant, 1995). Action potential prolongation in isolated papillary muscles depends on the orientation of the muscle (Knisley et al., 1992). Some of these results were predicted by the theory of an elongated cell in an electric field (Klee and Plonsey, 1976). A recent theoretical paper also showed correspondence between the Laplacian of extracellular potential and ΔV_m during bipolar stimulation (Muzikant and Henriquez, 1998), consistent with the conclusion that VG does not determine ΔV_m.

Limitations of the study

The model represented a two-dimensional sheet of myocardium, whereas the optical recordings were from the epicardium of three-dimensional rabbit heart. Thus the model reveals effects of fibers and electric field independent of the contribution of deeper layers in the heart wall to the epicardial V_m or extracellular voltage. In hearts, deeper layers may contribute; however, evidence indicates that this effect was small. Regarding epicardial ΔV_m, if deeper layers had a large effect, we would expect disagreement between the heart experiments and the model instead of the agreement seen in Figs. 2 and 6 and previously among hearts and two- and three-dimensional models (Sepulveda et al., 1989; Roth and Wikswo, 1994; Knisley, 1995). Furthermore, our unpublished simulation results demonstrate that changes in epicardial V_m in a three-dimensional bidomain model with fiber curvature are only slightly altered by fiber rotation in deeper layers, which agrees with results in the absence of fiber curvature (Muzikant and Henriquez, 1998). Regarding extracellular voltages, the effect of deeper layers that rotate counterclockwise (Streeter, 1979) may change the tilt of isovoltage lines for uniform S2 in hearts (Fig. 9). This can be demonstrated in a three-dimensional bidomain model with or without fiber curvature (our unpublished simulations and Muzikant and Henriquez, 1998) and may be due to the effect of fiber rotation on current in deeper layers (Baynham and Knisley, 1999). Our measurements indicate that this effect is minimal for nonuniform S2 (Figs. 3 and 7), which is consistent with current from the small epicardial electrode more concentrated near epicardium. The model of Muzikant and Henriquez (1998) predicted that epicardially determined Laplacians have opposite polarity along and across epicardial fibers, which agrees with our measurements. Moreover, our measurements did not miss epicardial VG in the depth direction because insulation was adjacent to the recording region.

Precision of fiber orientations in the model was limited because only macroscopic changes in fiber orientation were determined. However, hearts were moist and structurally intact, eliminating geometrical errors due to drying, cutting, or loss of reference to the apicobasal axis. Tissue inhomogeneities not included in the computer model, such as intracellular conductivity gradients along the fibers due to discrete cellular structure (Plonsey and Barr, 1986; Krassowska et al., 1987), distribution of clefts (Gillis et al., 1996; Fast et al., 1998), or changes in intracellular volume fraction (Fishler, 1998) may lead to localized ΔV_m. Despite the incompleteness of the model, agreement between experimental and model results indicates involvement of the fibrous organization of myocardium in the shock-induced ΔV_m.

CONCLUSIONS

This study examined epicardial transmembrane and extracellular voltages induced by uniform and nonuniform

shocks in rabbit hearts and in a computer model that incorporated the epicardial fiber structure. The ΔV_m and extracellular voltages during the shocks indicate that 1) the fiber structure influences the extracellular shock electric field and the distribution of ΔV_m. 2) The spatial variation of extracellular VG, and not VG itself, is a major determinant of ΔV_m for nonuniform shocks. For uniform shocks, both extracellular VG and, to a greater extent, its spatial variation influence ΔV_m.

Supported by National Institutes of Health grants HL52003 and RR11718; American Heart Association grant 9740173N; American Heart Association, Louisiana Affiliate grant 9820008LA; National Science Foundation grants DMF-9709754 and BES-9809132; and a contract LEQSF(1998-01)-RDA-A-30 from the Louisiana Board of Regents through the Board of Regents Support Fund. SBK is an Established Investigator Awardee of the American Heart Association.

REFERENCES

Baynham, T. C., and S. B. Knisley. 1999. Effective epicardial resistance of rabbit ventricles. *Ann. Biomed. Eng.* 27:96–102.

Beeler, G. W., and H. Reuter. 1977. Reconstruction of the action potential of ventricular myocardial fibres. *J. Physiol. (Lond.).* 268:177–210.

Clerc, L. 1976. Directional differences of impulse spread in trabecular muscle from mammalian heart. *J. Physiol. (Lond.).* 255:335–346.

Colli-Franzone, P., and L. Guerri. 1993. Models of the spreading of excitation in the myocardial tissue. *In* High-Performance Computing in Biomedical Research. T. C. Pilkington, B. Loftis, J. F. Thompson, S. L.-Y. Woo, T. C. Palmer, and T. F. Budinger, editors. CRC Press, Boca Raton, FL. 359–401.

Drouhard, J.-P., and F. A, Roberge. 1982. A simulation study of the ventricular myocardial action potential. *IEEE Trans. Biomed. Eng.* 29: 494–502.

Efimov, I. R., Y. N. Cheng, M. Biermann, D. R. Van Wagoner, T. N. Mazgalev, and P. J. Tchou. 1997. Transmembrane voltage changes produced by real and virtual electrodes during monophasic defibrillation shock delivered by an implantable electrode. *J. Cardiovasc. Electrophysiol.* 8:1031–1045.

Entcheva, E., J. Eason, I. Efimov, Y. Cheng, R. Malkin, and F. Claydon. 1998. Virtual electrode effects in transvenous defibrillation-modulation by structure and interface: evidence from bidomain simulations and optical mapping. *J. Cardiovasc. Electrophysiol.* 9:949–961.

Entcheva, E., N. A. Trayanova, and F. Claydon. 1999. Patterns of and mechanisms for shock-induced polarization in the heart: a bidomain analysis. *IEEE Trans. Biomed. Eng.* 46:260–270.

Fast, V. G., S. Rohr, A. M. Gillis, and A. G. Kleber. 1998. Activation of cardiac tissue by extracellular electrical shocks: formation of "secondary sources" at intercellular clefts in monolayers of cultured myocytes. *Circ. Res.* 82:375–385.

Fishler, M. G. 1998. Syncytial heterogeneity as a mechanism underlying cardiac far-field stimulation during defibrillation-level shock. *J. Cardiovasc. Electrophysiol.* 9:384–394.

Frazier, D. W., W. Krassowska, P.-S. Chen, P. W. Wolf, E. G. Dixon, W. M. Smith, and R. E. Ideker. 1988. Extracellular field required for excitation in three-dimensional anisotropic canine myocardium. *Circ. Res.* 63:147–164.

Frazier, D. W., P. D. Wolf, J. M. Wharton, A. S. L. Tang, W. M. Smith, and R. E. Ideker. 1989. Stimulus-induced critical point: mechanism for electrical initiation of reentry in normal canine myocardium. *J. Clin. Invest.* 83:1039–1052.

Gillis, A., V. Fast, S. Rohr, and A. G. Kleber. 1996. Spatial changes in transmembrane potential during extracellular electric shocks in cultured monolayers of neonatal rat ventricular myocytes. *Circ. Res.* 79: 676–690.

Henriquez, C. S. 1993. Simulating the electrical behavior of cardiac muscle using the bidomain model. *Crit. Rev. Biomed. Eng.* 21:1–77.

Hill, B. C., and K. R. Courtney. 1987. Design of a multi-point laser scanned optical monitor of cardiac action potential propagation: application to microreentry in guinea pig atrium. *Ann. Biomed. Eng.* 15: 567–577.

Holley, L. K., and S. B. Knisley. 1997. Transmembrane potentials during high voltage shocks in ischemic cardiac tissue. *PACE.* 20:146–152.

Ideker, R. E., A. S. L. Tang, D. W. Frazier, N. Shibata, P.-S. Cheng, and J. M. Wharton. 1991. Ventricular defibrillation: basic concepts. *In* Cardiac Pacing and Electrophysiology. N. El-Sherif and P. Samet, editors. W. B. Saunders, Orlando, FL. 713–726.

Klee, M., and R. Plonsey. 1976. Stimulation of spheroidal cells—the role of cell shape. *IEEE Trans. Biomed. Eng.* 23:347–354.

Knisley, S. B. 1995. Transmembrane voltage changes during unipolar stimulation of rabbit ventricle. *Circ. Res.* 77:1229–1239.

Knisley, S. B., and T. C. Baynham. 1997. Line stimulation parallel to myofibers enhances regional uniformity of transmembrane voltage changes in rabbit hearts. *Circ. Res.* 81:229–241.

Knisley, S. B., T. F. Blitchington, B. C. Hill, A. O. Grant, W. M. Smith, T. C. Pilkington, and R. E. Ideker. 1993. Optical measurements of transmembrane potential changes during electric field stimulation of ventricular cells. *Circ. Res.* 72:255–270.

Knisley, S. B., and A. O. Grant. 1995. Asymmetrical electrically induced injury of rabbit ventricular myocytes. *J. Mol. Cell. Cardiol.* 27: 1111–1122.

Knisley, S. B., and B. C. Hill. 1995. Effects of bipolar point and line stimulation in anisotropic rabbit epicardium: assessment of the critical radius of curvature for longitudinal block. *IEEE Trans. Biomed. Eng.* 42:957–966.

Knisley, S. B., B. C. Hill, and R. E. Ideker. 1994. Virtual electrode effects in myocardial fibers. *Biophys. J.* 66:719–728.

Knisley, S. B., W. M. Smith, and R. E. Ideker. 1992. Effect of field stimulation on cellular repolarization in rabbit myocardium: implications for reentry induction. *Circ. Res.* 70:707–715.

Krassowska, W., T. C. Pilkington, and R. E. Ideker. 1987. Periodic conductivity as a mechanism for cardiac stimulation and defibrillation. *IEEE Trans. Biomed. Eng.* 34:555–560.

LeGrice, I. J., B. H. Smaill, L. Z. Chai, S. G. Edgar, J. B. Gavin, and P. J. Hunter. 1995. Laminar structure of the heart: ventricular myocite arrangement and connective tissue architecture in the dog. *Am. J. Physiol.* 269:H571–H582.

Lepeschkin, E., H. C. Herrlich, S. Rush, J. L. Jones, and R. E. Jones. 1980. Cardiac potential gradients between defibrillation electrodes. *Med. Instrum.* 14:57 (Abstr.).

Lepeschkin, E., J. L. Jones, S. Rush, and R. E. Jones. 1978. Local potential gradients as a unifying measure for thresholds of stimulation, standstill, tachyarrhythmia and fibrillation appearing after strong capacitor discharges. *Adv. Cardiol.* 21:268–278.

Li, T., N. Sperelakis, R. E. Teneick, and R. J. Solaro. 1985. Effects of diacetyl monoxime on cardiac excitation-contraction coupling. *J. Pharmacol. Exp. Ther.* 232:688–695.

Mendenhall, W., R. L. Scheaffer, and D. D. Wackerly. 1986. Mathematical Statistics with Applications. Duxbury Press, Boston. 606–609.

Muzikant, A. L., and C. S. Henriquez. 1998. Bipolar stimulation of a three-dimensional bidomain incorporating rotational anisotropy. *IEEE Trans. Biomed. Eng.* 45:449–462.

Neunlist, M., and L. Tung. 1994. Optical recordings of ventricular excitability of frog heart by an extracellular stimulating point electrode. *PACE.* 17:1641–1654.

Neunlist, M., and L. Tung. 1995. Spatial distribution of cardiac transmembrane potentials around an extracellular electrode: dependence on fiber orientation. *Biophys. J.* 68:2310–2322.

Nielsen, P. M. F., I. J. LeGrice, B. H. Smaill, and P. J. Hunter. 1991. Mathematical model of geometry and fibrous structure of the heart. *Am. J. Physiol.* 260:H1365–H1378.

Plonsey, R., and R. C. Barr. 1986. Effect of microscopic and macroscopic discontinuities on the response of cardiac tissue to defibrillating (stimulating) currents. *Med. Biol. Eng. Comput.* 24:130–136.

Rattay, F. 1989. Analysis of models for extracellular fiber stimulation. *IEEE Trans. Biomed. Eng.* 36:676–682.

Roberts, D. E., and A. M. Scher. 1982. Effect of tissue anisotropy on extracellular potential fields in canine myocardium in situ. *Circ. Res.* 50:342–351.

Roth, B. J., and J. P. Wikswo, Jr. 1994. Electrical stimulation of cardiac tissue: a bidomain model with active membrane properties. *IEEE Trans. Biomed. Eng.* 41:232–240.

Sepulveda, N. G., B. J. Roth, and J. P. Wikswo, Jr. 1989. Current injection into a two-dimensional anisotropic bidomain. *Biophys. J.* 55:987–999.

Skouibine, K., N. A. Trayanova, and P. Moore. 1999. Anode/cathode make and break phenomena in a model of defibrillation. *IEEE Trans. Biomed. Eng.* 46:769–777.

Snyder, W. V. 1978. Algorithm 531 contour plotting. *ACM Trans. Math. Software.* 4:290–294.

Sobie, E. A., R. C. Susil, and L. Tung. 1997. A generalized activating function for predicting virtual electrodes in cardiac tissue. *Biophys. J.* 73:1410–1423.

Spach, M. S., and R. C. Barr. 1975. Ventricular intramural and epicardial potential distributions during ventricular activation and repolarization in the intact dog. *Circ. Res.* 37:243–257.

Streeter, D. D., Jr. 1979. Gross morphology and fiber geometry of the heart. *In* Handbook of Physiology, Section 2: The Cardiovascular System. R. M. Berne, N. Sperelakis, and S. R. Geiger, editors. American Physiological Society, Bethesda, MD. 61–112.

Trayanova, N. A. 1993. Transmembrane potential changes during stimulation in a bidomain model of the myocardium. *In* Computers in Cardiology. IEEE Computer Society Press, Los Alamitos, CA. 253–256.

Trayanova, N. A. 1996. Discrete versus syncytial tissue behavior in a model of cardiac stimulation. II. Results of simulation. *IEEE Trans. Biomed. Eng.* 43:1141–1150.

Trayanova, N. A., B. J. Roth, and L. J. Malden. 1993. The response of a spherical heart to a uniform electric field: a bidomain analysis of cardiac stimulation. *IEEE Trans. Biomed. Eng.* 40:899–908.

Trayanova, N. A., and K. Skouibine. 1998. Modeling defibrillation: effects of fiber curvature. *J. Cardiol.* 31(Suppl.):23–29.

Trayanova, N. A., K. Skouibine, and F. Aguel. 1998. The role of cardiac tissue structure in defibrillation. *Chaos.* 8:221–233.

Tung, L., N. Sliz, and M. R. Mulligan. 1991. Influence of the electrical axis of stimulation on excitation of cardiac muscle cells. *Circ. Res.* 69: 722–730.

Vetter, F. J., and A. D. McCulloch. 1998. Three-dimensional analysis of regional cardiac function: a model of rabbit ventricular anatomy. *Prog. Biophys. Mol. Biol.* 69:157–183.

Weidmann, S. 1970. Electrical constants of trabecular muscle for mammalian heart. *J. Physiol. (Lond.).* 210:1041–1054.

Wikswo, J. P., Jr., S.-F. Lin, and R. A. Abbas. 1995. Virtual electrodes in cardiac tissue: a common mechanism for anodal and cathodal stimulation. *Biophys. J.* 69:2195–2210.

Zhou, X., J. P. Daubert, P. D. Wolf, W. M. Smith, and R. E. Ideker. 1993. Epicardial mapping of ventricular defibrillation with monophasic and biphasic shocks in dogs. *Circ. Res.* 72:145–160.

Zhou, X., R. E. Ideker, T. F. Blitchington, W. M. Smith, and S. B. Knisley. 1995. Optical transmembrane potential measurements during defibrillation-strength shocks in perfused rabbit hearts. *Circ. Res.* 77:593–602.